

Initial Performance Outlook on the Sliding Particle Receiver (SlideRec)

Hicham Barbri¹, Derwalt J Erasmus¹, Alex Boman¹, Luka Lackovic^{1,*},
Martina Neises-von Puttkamer¹, and Reiner Buck¹

¹ DLR German Aerospace Center, Germany

* Correspondence: Luka Lackovic, luka.lackovic@dlr.de

Abstract. The next generation of central receivers is expected to reach high outlet temperatures of 800 °C and above, maintain stable operation and react to a varying incoming flux magnitude caused by hourly and seasonal variations, endure high-temperature operation, and remain cost-effective. Particle-based central receivers are being considered due to their high-temperature durability and favorable thermal properties of particle materials such as bauxite particles. This paper describes a new particle-based central receiver concept and provides an initial exploration of its performance in comparison with the existing CentRec[®] technology. Discrete Element Method (DEM) simulations demonstrated that a stable falling and sliding particle film can be achieved inside the SlideRec. The residence time of particle flow within the SlideRec is estimated to be higher than a falling particle receiver and similar to that of an obstructed-flow receiver. The results of the thermal model (incorporating reflective, radiative, convective and conductive heat losses) indicate that the SlideRec demonstrates a higher thermal efficiency than the CentRec[®] under an incoming aperture flux of between 0.1 MW/m² and 1.7 MW/m². The concept therefore is promising and is recommended for further experimental exploration.

Keywords: Central Receiver, Particles, Direct Absorption Receiver, Falling Particle Film, Granular Flow on an Inclined Surface

1. Introduction

Simplicity and low production costs were the motivational factors for the development of a new particle central receiver with no moving parts. The low complexity is also expected to enable robust operation. The SlideRec receiver concept employs an internal falling particle curtain with a subsequent sliding particle film. Previous particle-based central receiver concepts based on a sliding particle film, also known as granular flow over an inclined surface, have been investigated in [1], [2], [3]. A concept sketch of the SlideRec concept is presented in Figure 1. The receiver consists of a box-like cavity (inclined at around $30^\circ - 45^\circ$) with an internal-angled falling particle film entering the cavity alongside its back face. The film falls onto the bottom face of the box where it mixes and subsequently proceeds, by sliding over an inclined surface, towards the aperture of the cavity where it exits into an outlet hopper.

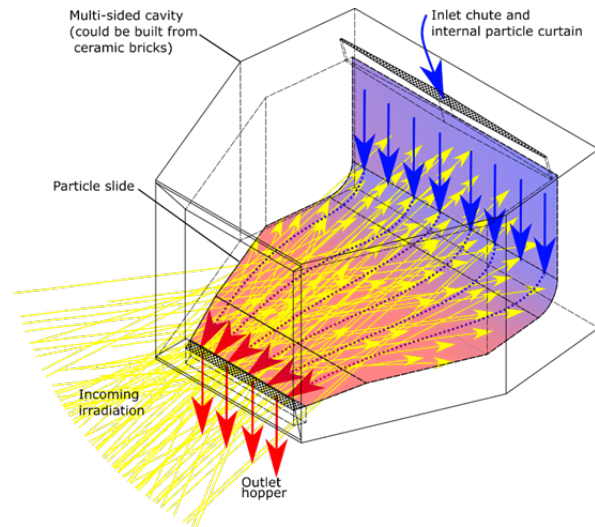


Figure 1. Diagram of the SlideRec central receiver concept

Achieving a high residence time can enable reaching higher outlet temperatures. In general, the residence of a particle receiver can be increased by introducing obstructions, a sliding surface or simply by dimensional up-scaling. In the case of the SlideRec, it can be manipulated by modifying the tilt angle, the dimensions as well as by incorporating obstructions. The SlideRec can also be controlled to account for a changing incoming flux magnitude by controlling the inlet particle mass flow rate with a variable orifice or a slide gate.

Inside the cavity, the back wall is substantially shielded from incoming irradiation by the falling particle film and the bottom (sliding) surface is shielded by stationary, sliding and rolling particles. However, the side walls and the top wall are exposed to incoming irradiation, these surfaces are therefore coated with a reflective surface to reflect incoming radiation towards the particles and also out of the aperture.

2. Discrete Element Method (DEM) investigation

A DEM investigation was conducted in order to iterate the design to achieve uniform flow over the sliding surface and also to estimate the residence time of particles through the domain. The scale of the aperture is $1\text{ m} \times 1\text{ m}$ to enable comparability to previous on-sun tests by [4] and [5]. An inclination angle of 40° was chosen with a mass flow rate of 6.41 kg/s . This is about the required flow rate to achieve a 325 K temperature increase for particles collecting 2.5 MW/m^2 of flux. The DEM model was based on the model developed by [6]. The elastic-plastic spring-dashpot (EPSD2) rolling friction model was employed with the hertz granular model. A timestep of $1\text{e-}5\text{ s}$ was chosen for this particle size. A particle neighbor cut-off distance of 1 particle diameter was simulated. The following properties were assumed:

- Particle type: Saint Gobain SG10H,
- Particle diameter: 1.2 mm ,
- Particle density: 3560 kg/m^3 ,
- Youngs modulus: 5 MPa ,
- Poisson ratio: 0.3 ,
- Particle-particle restitution coefficient, e_{pp} : 0.46 ,

- Particle-wall restitution coefficient, e_{pw} : 0.43,
- Particle-particle sliding friction coefficient, μ_{pp} : 0.53,
- Particle-particle rolling friction coefficient, $\mu_{R,pp}$: 0.16,
- Particle-wall sliding friction coefficient, μ_{pw} : 1.00,
- Particle-wall rolling friction coefficient, μ_{RpW} : 1.00.

The particle-wall friction factors were set to 1 to approximate an arbitrarily rough surface and enable a stationary base layer of particles. The stationary base layer is expected to enable reduced thermal stress on the receiver due to lower surface temperatures.

Figure 2 demonstrates that a stable particle film can be achieved on the sliding surface and an angled, stable, falling film can be achieved along the back surface. The inlet chute cross-sectional area can be shaped by a diamond-like hexagonal shape increasing in width towards its centre as shown in Figure 1 and demonstrated in Figure 2 in order to balance the density distribution of the film with an incoming flux distribution. The falling film can also be aimed towards the back wall so that the particles collide with the back surface to further increase the residence time and improve mixing and homogenization of particle flow temperature. Figure 2 also shows that the particle surface velocity magnitude is almost an order of magnitude less than the falling film alongside the back surface.

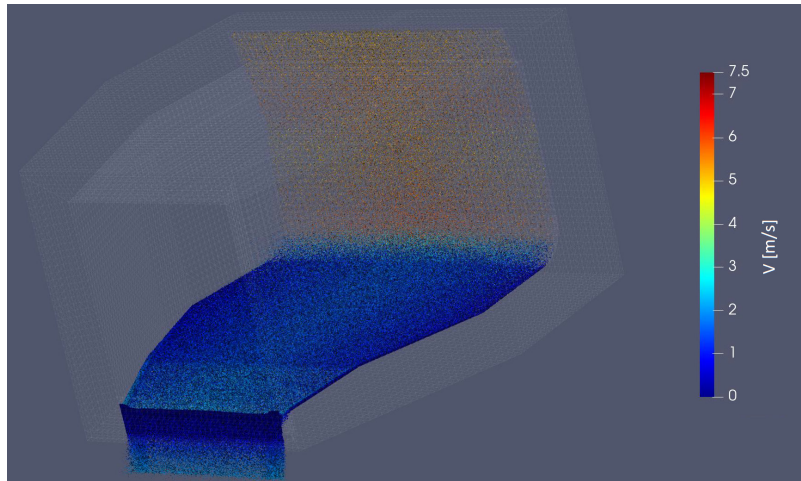


Figure 2. DEM snapshot depicting particle flow through the domain colored by velocity magnitude

Table 1 shows the estimated residence time of the SlideRec with a tilt angle of 40° compared to previous experimentally-tested concepts. The residence time of the CentRec with a 1 m^2 aperture was estimated analytically with the assumptions of a radial velocity gradient of $50 \frac{\text{m}}{\text{s}}/\text{m}$ and a 40% circumferential moving zone ratio. The DEM simulations demonstrate that for a similar aperture size, the residence time of the SlideRec is higher than that of a falling-particle receiver and similar to that of an obstructed-flow receiver.

Table 1. Residence time comparison with existing particle receivers

| Particle Receiver | Institution | Test year | Aperture size | Residence time range | Source |
|-------------------|----------------------|------------|-----------------|----------------------|--------|
| Free-falling | Sandia | 2015 | 1 m x 1 m | 0.2 ~ 0.4 s/m | [4] |
| Obstructed-flow | Sandia | 2015 | 1 m x 1 m | 1 ~ 3 s/m | [4] |
| Obstructed-flow | King Saud University | 2018 | [–] m x 1 m | 1.1 ~ 1.4 s/m | [5] |
| Centrifugal | DLR | Simulation | 1 m^2 | 24 s (controllable) | [-] |
| SlideRec | DLR | Simulation | 1 m x 1 m | 2 s/m | [-] |

3. Thermo-optical Model

For the overall thermodynamic analysis of a CSP plant, knowing the receiver's thermal efficiency is of importance. It is also of interest to model the surface temperature distribution of the receiver and particles to understand whether the required outlet temperature can be achieved and whether the exposed internal walls do not overheat under the concentrated incoming flux. In order to characterize the thermal performance of the SlideRec concept, a coupled three-dimensional steady-state thermal receiver model and a raytracing model of the heliostat, tower and receiver system is developed. The three basic thermal losses: radiation, conduction, and convection, as well as optical reflective losses, are incorporated. This model has already been validated using the experimental data from a CentRec test campaign [7].

3.1 Raytracing model

Optical ray-tracing simulation tools: FEMRAY [8] and SPRAY [9] are employed to model the incoming irradiance from the heliostats. These tools make use of a discretized surface mesh of the receiver to model the incoming flux distribution developed by the heliostat field on the discretized surface. The reflected radiation losses from the receiver surface are also modelled with the assumption of absorptivity (α) constants on the surfaces depicted in Figure 3. The DLR's heliostat field in Julich is modelled at 12 pm on March 21. The receiver height is 40 m and the inclination angle is 40°.

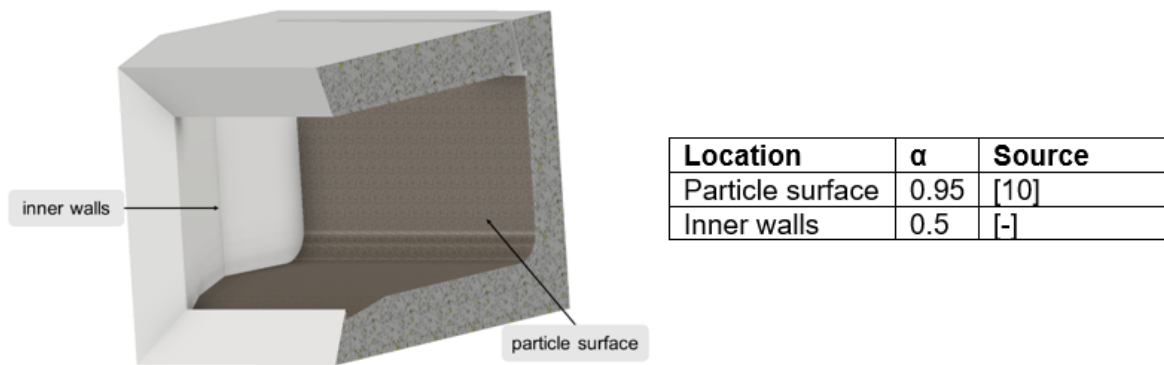


Figure 3. Section depicting the absorptivity (α) of the particle surface and inner walls

3.2 Numerical receiver model

A Finite Element Method (FEM) thermal model developed in ANSYS Mechanical is described and its basic structure and the applied boundary conditions are detailed. By the assumption of Kirchhoff's law of thermal radiation ($\alpha = \epsilon$), the incoming surface radiation after reflectance (output of the raytracing model) represents the input of the thermal model. This model simulates the three thermal losses: radiative, convective and conductive losses as well as the heat absorbed by the particle film.

Since the interaction of individual particles is not of interest for the present simulation, the ideal case is assumed, in which the particle surface is completely covered with an optically thick, homogeneous, 1D moving particle film. The heat transfer to the particles as well as the particle flow is modeled using a 1D discretized fluid line segment, called the fluid-flow line in ANSYS Mechanical. The discrete elements of the 1D line segment are thermally coupled to all the nearest surface elements on the allocated particle surface as depicted in Figure 4. Moreover, the modelled fluid flow follows the line segment from start to end and absorbs the (after reflection) flux imposed (after subsequent radiative, convective, and conductive losses) on the 3D surface elements as it proceeds in the direction of the line. The yellow lines in Figure 4 depict the connection of each fluid-flow line element to all nearest 3D surface elements.

Since the particle flow is modelled as fluid flow in ANSYS Mechanical, the incoming flux boundary condition must be modelled with a convective heat transfer coefficient between the particle surface elements and the fluid-flow line segment. In order to approximate direct absorption and re-radiation (after reflection), an almost infinite heat transfer coefficient of $10000 \text{ W}/(\text{m}^2\text{K})$ is assumed [7]. The particle material properties [10], particle mass flow and particle inlet temperature are assigned to the fluid line and are depicted in Table 2. The inlet temperature of the particles is a boundary condition and the resulting fluid-flow particle outlet temperature is the output-parameter.

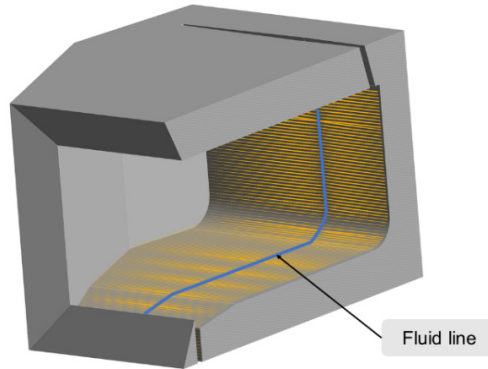


Figure 4. 1D fluid line with element-wise connections to the particle surface (yellow lines)

For the simulation of convective losses inside the cavity to the environment, the modified Clausen model was used [11]. The model calculates the convective losses to the environment of an inclined cavity as a function of its dimensions, the wind speed, the inclination angle, and internal wall temperature. Considering the applied temperature difference between ambient air and the cavity inner surface, a convective heat transfer coefficient is the output parameter. Based on an exploration of this model, an internal convective heat transfer coefficient of $2 \text{ W}/(\text{m}^2\text{K})$ is assumed [7].

The radiative heat transfer between the cavity's internal surfaces to neighboring internal surfaces as well as the ambient-temperature aperture are calculated using the radiosity method. The internal cavity is defined as a perfect thermal envelope. The inner surfaces are assumed as gray Lambertian surfaces. Based on solar absorptivity measurements, the particle surface is assigned a weighted hemispherical absorptivity of 0.95 [10]. Since the inner walls are intended to reflect radiation to remain cool, a reflective material of calotte foil is chosen on this surface to reflect the radiation as much as possible. Due to the reflective surface of this material, a weighted hemispherical absorptivity and emissivity of 0.5 is assumed. Alternative materials such as FiberFrax can also be used. The aperture is given an absorptivity and emissivity of 1 at a constant temperature of $25 \text{ }^\circ\text{C}$ to assume that all radiation from internal surfaces to the aperture are absorbed by the environment.

The losses due to conduction through the shell of the cavity are modeled by applying a temperature boundary condition to the outer walls of the receiver. The material of the shell is Microtherm, the thickness is 200 mm. For a conservative estimation, a rather low outer wall temperature of 25°C is assumed (equal to ambient temperature). The following table summarizes the boundary conditions.

Table 2. Boundary conditions and assumptions of the thermal FEM model

| Description | Value/Range | Unit |
|--|-------------|----------------------|
| Aperture temperature | 25 | [°C] |
| Ambient temperature | 25 | [°C] |
| Particle inlet temperature | 25 | [°C] |
| Internal cavity convective heat transfer coefficient | 2 | W/(m ² K) |
| Emissivity of the Inner walls | 0.5 | [-] |
| Emissivity of particle surface | 0.95 | [-] |
| Particle mass flow rate | 0.1 .. 1.3 | [kg/s] |
| Incoming aperture flux average magnitude | 0.1 .. 3.0 | MW/(m ²) |

The receiver thermal efficiency is determined by the ratio of the absorbed solar radiation (\dot{Q}_{abs}) of the particles and the incoming aperture flux (\dot{Q}_{in}):

$$\eta_{\text{th}} = \frac{\dot{Q}_{\text{in}} - \dot{Q}_{\text{ref}} - \dot{Q}_{\text{rad}} - \dot{Q}_{\text{conv}} - \dot{Q}_{\text{cond}}}{\dot{Q}_{\text{in}}} = \frac{\dot{Q}_{\text{abs}}}{\dot{Q}_{\text{in}}} \quad (1)$$

4. Results

Figure 5 demonstrates the incoming flux distribution alongside the internal surface temperature distribution. It is shown that the peak flux magnitude occurs on the bottom surface with a reduced flux magnitude on the back region and the side walls. The internal geometry's dimensions and the tilt angle can be modified to achieve a desired flux distribution. The target outlet temperature of 650 °C is achieved at an incoming flux magnitude of 1.5 MW/m². It is depicted that the exposed side walls and the top wall are maintained at a temperature below 1500 °C. This is a rather high peak temperature and further work should explore alternative geometric manifestations to reduce this peak. For example, 'FiberFrax' (ceramic fiber and aluminum silicate wool) has a temperature resistance up to around 1250 °C.

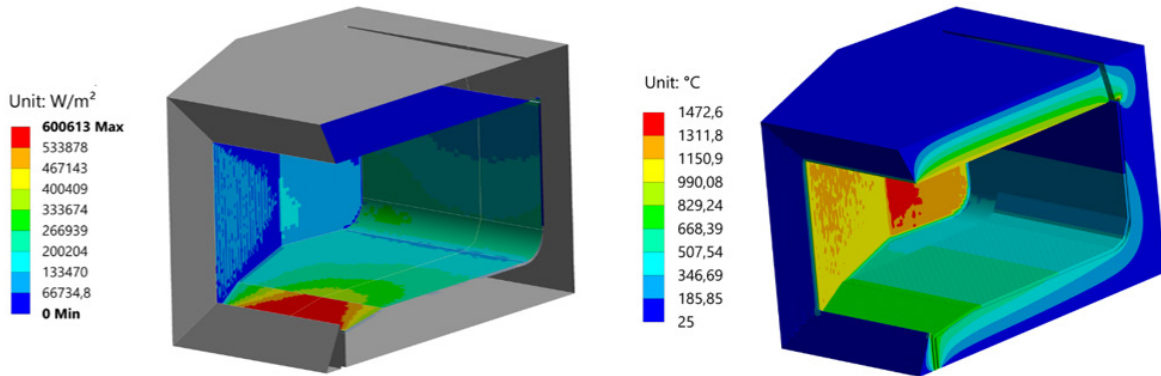


Figure 5. Local absorbed heat flux (left), temperature distribution on the SlideRec (right)

Figure 6 depicts the relative weightings of optical and thermal losses relative to the incoming and absorbed heat. It is shown that a major part of the incoming flux is absorbed by the particles. The most significant heat loss is the radiative loss. It is shown that the incident radiation is higher than the sum of the absorbed heat and the thermal losses by 2.7%. This is due to the uncertainty of the thermal model.

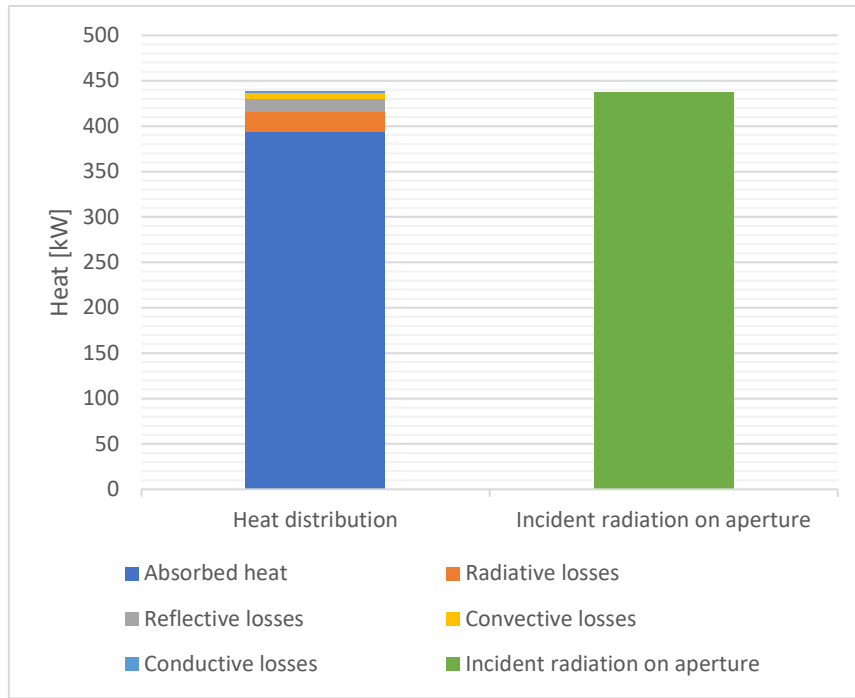


Figure 6. Comparison of incoming radiation with the absorbed heat and various thermal losses

Figure 7 depicts the effect of a varying incoming flux magnitude on the thermal efficiency. A range of incoming flux magnitudes were simulated with the mass flow rate constrained in each to reach an outlet temperature of 650 °C.

In Figure 7, the comparison expands to a simulated datapoint of the CentRec and the SlideRec along with a range of estimated datapoints based on the Constant Heat Loss Assumption (CHLA). Moreover, the assumption is that the inlet and outlet temperature are constrained (by choosing the correct mass flow rate to accompany the incoming flux magnitude), thus the average temperature inside the cavity should be similar and thereby independent of the incoming flux and it follows that the thermal losses should also be similar. It can be observed that the CHLA assumption for the SlideRec is substantially incorrect at lower fluxes. This is understood to be because the temperature of the side walls and the top wall cannot be constrained by the inlet and outlet particle temperature because they are directly exposed to incoming irradiation. The uncertainty is not expected to be as significant for the CentRec because the entire internal cylindrical surface of the CentRec is intended to be covered by a particle film and this is most of the surface area inside the cavity.

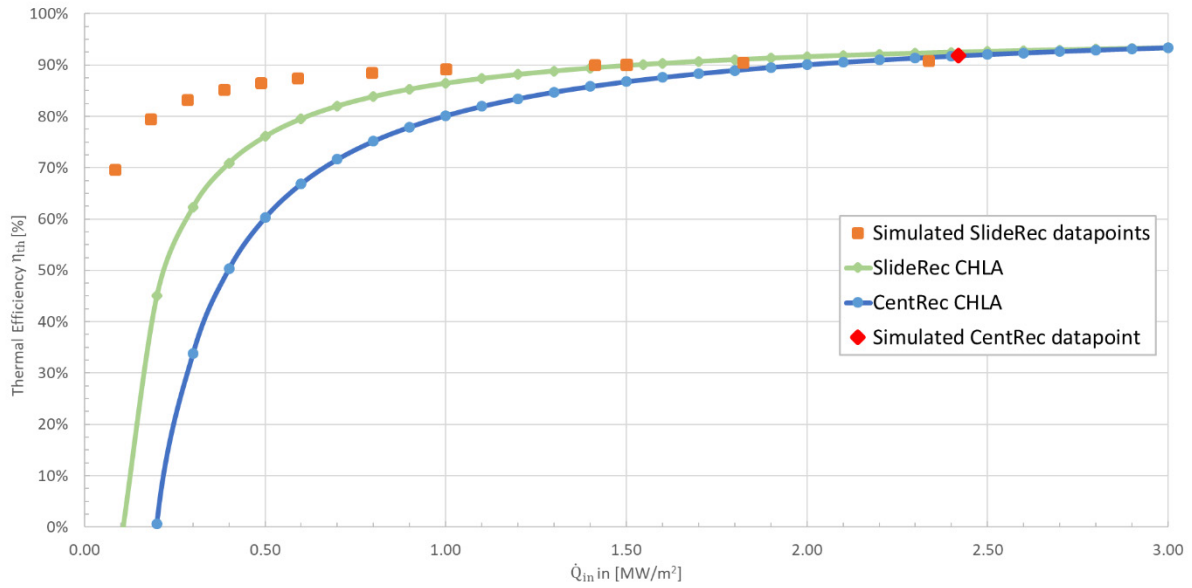


Figure 7. Thermal Efficiency distribution of several simulated SlideRec data points as well as a comparison between the CentRec [7] and the SlideRec based on a Constant Heat Loss Assumption (CHLA)

Comparing the thermal efficiency of the SlideRec and the CentRec, it is depicted that the SlideRec (CHLA) demonstrates a higher thermal efficiency than the CentRec (CHLA) under simulated incoming flux magnitudes below 2 MW/m². At flux magnitudes over 2 MW/m², the thermal efficiency is similar for both concepts. The simulated data points of the SlideRec (without the CHLA) depict a higher thermal efficiency than the CentRec CHLA under an incoming aperture flux of between 0.1 MW/m² and 1.7 MW/m². This finding is promising for the future potential development of the SlideRec. It must be noted that this is a simulation and the findings on the SlideRec have not yet been validated experimentally.

5. Conclusion and Outlook

The DEM simulations demonstrated that a stable particle film can be achieved on the sliding surface of the SlideRec and an angled, stable falling film can be achieved along the back surface. The residence time of particle flow within the SlideRec is estimated to be higher than that of a falling particle receiver and similar to that of an obstructed-flow receiver. The thermal analysis indicates that at flux levels between 0.1 MW/m² and 1.7 MW/m², the SlideRec demonstrates a higher thermal efficiency than the CentRec. At flux magnitudes over 2 MW/m², the thermal efficiency is similar for both concepts. This is a promising result and prompts further exploration of the SlideRec. However, it must be noted that in this study, the findings are based on simulation and an experimental campaign will be necessary in the future to validate these findings. Further work should include developing and exploring the granular flow behaviour of an experimental SlideRec prototype and investigating the controllability of the residence time and flow rate to compensate a cycling incoming flux magnitude over the course of a day and year. Future work can include on-sun testing of the concept.

Data availability statement

Non-confidential data can be provided by the corresponding author upon request.

Author contributions

Hicham Barbri: formal analysis, data curation, writing – original draft; Derwalt J Erasmus: conceptualization, methodology, data curation, formal analysis, software, writing – review and editing, visualization; Alex Boman: data provision, writing – review and editing; Reiner Buck: data provision, writing – review and editing.

Competing interests

The authors declare that they have no competing interests.

Funding

This work was funded internally with DLR e.V. funds.

References

- [1] S. Möller, R. Palumbo. "The Development of a Solar Chemical Reactor for the Direct Thermal Dissociation of Zinc Oxide" *Journal of Solar Energy Engineering*, vol. 123 (2001)
- [2] X. Xie, G. Xiao, M. Ni, J. Yan, H. Dong, K. Cen, "Optical and thermal performance of a novel solar particle receiver", *SolarPACES 2018, Casablanca, Morocco* (2019).
- [3] A. J. Schrader, G. L. Schieber, A. Ambrosini, P. G. Loutzenhiser, "Experimental demonstration of a 5 kWth granular-flow reactor for solar thermochemical energy storage with aluminum-doped calcium manganite particles" *Applied Thermal Engineering*, vol. 173 (2020) 115257.
- [4] C.K. Ho, J.M. Christian, J.E. Yellowhair, K. Armijo, W.J. Kolb, S. Jeter, M. Golob, C. Nguyen, "On-Sun Performance Evaluation of Alternative High-Temperature Falling Particle Receiver Designs". *Journal of Solar Energy Engineering*, vol. 141 (2019) 011009-1.
- [5] H. Al-Ansary, A. El-Leathy, A. Alswaiyd, S. Alaqel, N. Saleh, R. Saeed, Z. Al-Suhaibani, S. Danish, E. Djajadiwinata, and S. Jeter, "Study of the optimum discrete structure configuration in obstructed flow particle heating receivers", *AIP Conference Proceedings* 2303, 030001 (2020).
- [6] J. Grobbel, "Modeling Solar Particle Receivers with the Discrete Element Method", PhD Thesis, RWTH Aachen, Germany (2019).
- [7] C. Frantz, M. Ebert, L. Amsbeck, "Experimental Evaluation of the Thermo-Optical Efficiency of a Centrifugal Particle Receiver", *ASME 2019 - 13th International Conference on Energy Sustainability ES 2019, Phoenix, AZ, USA*.
- [8] R. Uhlig, "FEMRAY User's Manual", DLR, Stuttgart, Germany, 2010.
- [9] R. Buck, "Solar Power Raytracing Tool SPRAY", User Manual, Version 17, 19/06/2016
- [10] G. Alkan, P. Mechnich, H. Barbri, F. Flucht, J. Pernpeintner, D. Sergeev, M. Müller, "Evaluation of Ceramic Proppants as Heat Transfer and Storage Medium". *SolarPACES 2021*, online, in print.
- [11] A. M. Clausing, J. M. Waldvogel, and L. D. Lister, "Natural Convection from Isothermal Cubical Cavities with a Variety of Side-facing Apertures", *J. Heat Transfer*, vol. 109, pp. 407–412, 1987.